

Propagation, generation, and utilization of topologically trivial magnetic solitons in magnetic nanowires

Kai-Tao Huang(黄铠涛) and X. S. Wang(王宪思)

Citation: Chin. Phys. B, 2025, 34 (**10**): 107502. DOI: 10.1088/1674-1056/adf4ab
http://cpb.iphy.ac.cn; http://iopscience.iop.org/cpb

What follows is a list of articles you may be interested in

Direct observation of ultrafast magnetization dynamics in Co/Ni bit patterned media by time-resolved scanning Kerr microscopy

Wei Zhang(张伟), Wei He(何为), Qin-Li Lv(吕琴丽), Jian-Wang Cai(蔡建旺), Xiang-Qun Zhang(张向群), and Zhao-Hua Cheng(成昭华)
Chin. Phys. B, 2025, 34 (**4**): 047501. DOI: 10.1088/1674-1056/adb67e

Thickness-dependent magnetic properties in Pt/[Co/Ni]$_n$ multilayers with perpendicular magnetic anisotropy

Chunjie Yan(晏春杰), Lina Chen(陈丽娜), Kaiyuan Zhou(周恺元), Liupeng Yang(杨留鹏), Qingwei Fu(付清为), Wenqiang Wang(王文强), Wen-Cheng Yue(岳文诚), Like Liang(梁力克), Zui Tao(陶醉), Jun Du(杜军),Yong-Lei Wang(王永磊), and Ronghua Liu(刘荣华)
Chin. Phys. B, 2023, 32 (**1**): 017503. DOI: 10.1088/1674-1056/ac5c37

Observation of nonlinearity and heating-induced frequency shifts in cavity magnonics

Wei-Jiang Wu(吴维江), Da Xu(徐达), Jie Qian(钱洁), Jie Li(李杰), Yi-Pu Wang(王逸璞), and Jian-Qiang You(游建强)
Chin. Phys. B, 2022, 31 (**12**): 127503. DOI: 10.1088/1674-1056/ac9b02

Antiferromagnetic spin dynamics in exchanged-coupled Fe/$GdFeO_3$ heterostructure

Na Li(李娜), Jin Tang(汤进), Lei Su(苏磊), Ya-Jiao Ke(柯亚娇), Wei Zhang(张伟), Zong-Kai Xie(谢宗凯), Rui Sun(孙瑞), Xiang-Qun Zhang(张向群), Wei He(何为), and Zhao-Hua Cheng(成昭华)
Chin. Phys. B, 2021, 30 (**11**): 117502. DOI: 10.1088/1674-1056/abf3b7

Interaction region of magnon-mediated spin torques and novel magnetic states

Zai-Dong Li(李再东), Qi-Qi Guo(郭奇奇), Yong Guo(郭永), Peng-Bin He(贺鹏斌), and Wu-Ming Liu(刘伍明)
Chin. Phys. B, 2021, 30 (**10**): 107506. DOI: 10.1088/1674-1056/ac04a8

SPECIAL TOPIC — Advanced magnonics

Propagation, generation, and utilization of topologically trivial magnetic solitons in magnetic nanowires

Kai-Tao Huang(黄铠涛) and X. S. Wang(王宪思)†

School of Physics and Electronics, Hunan University, Changsha 410082, *China*

(Received 1 April 2025; revised manuscript received 24 July 2025; accepted manuscript online 28 July 2025)

Magnetic solitons are nonlinear, local excitations in magnetic systems. In this study, we theoretically and numerically investigate the properties and generation of one-dimensional (1D) topologically trivial magnetic solitons in ferromagnetic nanowires. An approximate analytical soliton solution described by two free parameters is validated by comparison with the micromagnetic simulation. Across an interface between two media of different anisotropy, the reflection and refraction of a soliton are highly nonlinear, which differ from linear spin waves. A pair of magnetic solitons that propagate in opposite directions can be generated by alternately applying magnetic-field or spin-polarized-current pulses of opposite directions to at least two successive regions. Each soliton corresponds to a soliton solution that can be controlled by the generation process. These magnetic solitons can be used to drive domain wall motion over a distance determined by the soliton magnitude, allowing for discrete manipulation of domain walls compatible with the digital nature of information technology. Our findings pave the way for the application of topologically trivial solitons in spintronics.

Keywords: magnetization dynamics, soliton, nonlinear dynamics

PACS: 75.78.–n, 05.45.Yv

DOI: 10.1088/1674-1056/adf4ab **CSTR:** 32038.14.CPB.adf4ab

1. Introduction

Over the past few decades, spintronic devices have attracted much attention due to their low power consumption and non-volatile storage capabilities.[1–3] Some prototype devices, such as racetrack memories[4,5] and magnetic logic gates,[6–8] have been experimentally demonstrated. From both practical and academic perspectives, the properties and manipulation of magnetic solitons have garnered considerable interest. Magnetic solitons are localized, nonlinear solutions of the magnetization dynamic equation that can maintain their shape and velocity, in contrast to linear wave packets that suffer dispersion during propagation.[9] Magnetic solitons can be categorized based on the winding number of the magnetization in space, which serves as a topological invariant.[10] Intensive studies have focused on topologically nontrivial solitons, such as domain walls, skyrmions, and hopfions, due to their exotic structures and potential applications.[11–17] The nontrivial topology of solitons usually implies enhanced stability of the soliton textures, making them suitable for non-volatile data carriers. However, it is also a double-edged sword, as it introduces drawbacks such as unexpected Hall effects[18] and difficulty in creation.[19,20]

In contrast, topologically trivial magnetic solitons are far less studied. Distinct from their topological counterparts, topologically trivial solitons in magnetic systems are solitary waves that are easy to create and annihilate, referred to as magnetic drops,[21] magnetic droplets,[22] or simply magnetic solitons if there is no ambiguity in the context.[23] Up to now, most studies have focused on magnetic solitons in one-dimensional (1D) and two-dimensional (2D) systems. In 2D, the magnetic soliton can be created by using spin-transfer torque beneath a nanocontact on a ferromagnetic film with perpendicular magnetic anisotropy (PMA).[24,25] The 2D magnetic soliton is usually generated locally and used as a nano-oscillator.[26] Investigations on 1D magnetic solitons in ferromagnetic nanowires mainly focus on their analytical solutions and propagation.[27–32] However, many issues remain unsolved, mainly due to the complexity and nonlinearity of the Landau–Lifshitz–Gilbert (LLG) equation governing the magnetization dynamics. It is difficult to obtain exact analytical solutions for magnetic solitons even in the simplest 1D case, so some approximations are necessary. The inhomogeneous demagnetization field is often ignored, and the dissipationless part of the LLG equation can be transformed into the nonlinear Schrödinger equation by retaining the cubic order of the soliton amplitude, allowing analytical soliton solutions to be obtained.[27–32] However, the validity of these approximations has not been fully justified; in other words, whether the analytical solutions remain valid in the presence of the intact demagnetization field and damping is not clear. How solitons reflect at an interface between two nanowires with different material parameters is also unknown. Furthermore, there is no systematic way to generate a specific soliton mode in a 1D nanowire

†Corresponding author. E-mail: justicewxs@hnu.edu.cn

© 2025 Chinese Physical Society and IOP Publishing Ltd. All rights, including for text and data mining, AI training, and similar technologies, are reserved.

yet.

In this paper, we first verify the validity of the analytical soliton solution[23,27] in the presence of the full demagnetization field, nonlinear effects, and Gilbert damping by numerical simulation of the LLG equation starting from a certain solution. We find that for small soliton amplitudes and low damping ($\sim 10^{-4}$), the analytical solution agrees well with the numerical results. When the soliton amplitude grows larger, the soliton speed becomes slower than that predicted by the initial analytical solution. For a nanowire consisting of two segments with different anisotropies, the reflection and refraction of an incident soliton are complicated and differ from those of linear spin waves. The soliton undergoes total refraction (reflection) when propagating into a medium with weak (strong) anisotropy, while refraction and reflection coexist at intermediate anisotropy. Then, we design a method for generating magnetic solitons in a uniform domain by applying stimuli (magnetic field or spin-polarized current pulses) to at least two successive regions. The directions of the stimuli in adjacent regions should be opposite. Two magnetic solitons are generated as a pair and correspond to the two soliton solutions mentioned above. The properties of the generated solitons can be tuned by the strength and width of the stimulated regions. When a magnetic soliton passes through a domain wall, the domain wall shifts by a distance toward the opposite direction of the soliton propagation because of angular momentum conservation.[33] The distance depends on the amplitude of the magnetic soliton. This procedure can be repeated to realize discrete manipulation of domain walls, which is highly compatible with the digital nature of information storage and transmission.

2. Model and results

2.1. Analytical solution of solitons and numerical verification

A ferromagnetic nanowire with saturation magnetization M_s along the x direction is considered. An easy-axis anisotropy along the wire maintains a single-domain ground state of $m_x = \pm 1$. We also allow an external field $\boldsymbol{B}_0 = B_0\hat{\boldsymbol{x}}$ to be applied along the wire. A magnetic soliton is a solitary excitation on the single-domain ground state, in contrast to a domain wall, which represents the transition region between two opposite domains, as illustrated in Fig. 1(a). The LLG equation reads

$$\frac{\partial \boldsymbol{m}}{\partial t} = -\gamma \boldsymbol{m} \times \boldsymbol{B}_{\text{eff}} + \alpha \boldsymbol{m} \times \frac{\partial \boldsymbol{m}}{\partial t}, \tag{1}$$

where $\boldsymbol{m}$ is the unit vector of the magnetization field whose saturation magnitude is $M_s = 0.86 \times 10^6$ A/m, $\gamma = 28$ GHz/T is the gyromagnetic ratio, and α is the Gilbert damping. $\boldsymbol{B}_{\text{eff}}$ is the effective field, consisting of the exchange field $\frac{2A}{M_s}\frac{\partial^2 \boldsymbol{m}}{\partial x^2}$ (with exchange constant A), the anisotropy field $\frac{2K}{M_s} m_x \hat{\boldsymbol{x}}$, the external field $B_0\hat{\boldsymbol{x}}$, and the demagnetization field $\boldsymbol{B}_{\text{d}}$.

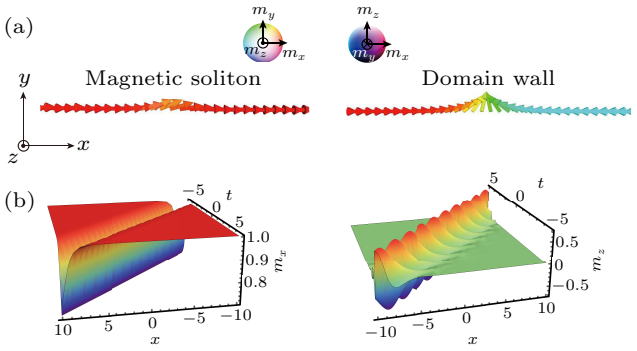


Fig. 1. (a) Illustration of magnetization profiles of a typical magnetic soliton (left) and a head-to-head domain wall (right), with arrows denoting local magnetization directions. The color scheme is shown in the inset. (b) 3D plot of the analytical solutions for the m_x and m_z components in the x–t plane.

The analytical solution of the solitons is obtained under the following assumptions: (i) the demagnetization field $\boldsymbol{B}_{\text{d}}$ is approximated by the shape anisotropy of an infinite rod, $\boldsymbol{B}_{\text{d}} = \frac{1}{2}\mu_0 M_s m_x \hat{\boldsymbol{x}}$; (ii) the damping term can be ignored; and (iii) the deviation of $\boldsymbol{m}$ from the x direction is small.[23,27–32] To simplify the expressions, spatial unit $x_0 = \sqrt{2A/(\mu_0 M_s^2)}$, temporal unit $t_0 = (\gamma\mu_0 M_s)^{-1}$, and field unit $\mu_0 M_s$ are used to define dimensionless variables and parameters $x' = (x - X_0)/x_0$, $t' = (t - T_0)/t_0$, $\lambda = 2K/(\mu_0 M_s^2)$, and $b_0 = B_0/(\mu_0 M_s)$. Here X_0 and T_0 are certain initial position and time, respectively. By defining $\psi = m_y - \mathrm{i}m_z$ and retaining the cubic terms of ψ, we obtain a Schrödinger equation with both linear and nonlinear terms

$$\begin{aligned} \mathrm{i}\frac{\partial \psi}{\partial t'} = &-\frac{\partial^2 \psi}{\partial x'^2} + \left(b_0 + \lambda + \frac{1}{2}\right)\psi \\ &-\frac{1}{2}\left(\lambda + \frac{1}{2}\right)|\psi|^2\psi = 0. \end{aligned} \tag{2}$$

When $b_0 + \lambda + \frac{1}{2} = 0$, the remaining term corresponds to a pure nonlinear Schrödinger equation, one of whose soliton solutions can be obtained by the Hirota method.[23,29,34] Otherwise, the linear term introduces an additional precession frequency around the x direction. Except for arbitrary initial position X_0 and time T_0, the exact solutions of Eq. (2) are determined by only two free parameters, a and b, as

$$\begin{aligned} \psi(x',t') = &\, C(a)\,\mathrm{e}^{\mathrm{i}[bx' - \omega_0(a,b)t']} \\ &\times \mathrm{sech}[a(x' - 2bt') - \ln 2C(a)], \end{aligned} \tag{3}$$

where $C(a) = \frac{2a}{\sqrt{\lambda + 1/2}}$ and $\omega_0 = h_0 + \lambda + \frac{1}{2} - (a^2 - b^2)$. Physically, this solution consists of an oscillatory part $\mathrm{e}^{\mathrm{i}[bx' - \omega_0(a,b)t']}$ with a precession frequency ω_0/t_0 and "wavelength" $2\pi x_0/b$, and an envelope $C(a)\mathrm{sech}[a(x' - 2bt') - \ln 2C(a)]$ with amplitude $C(a)$ and propagation speed $2bv_0$ ($v_0 = x_0/t_0$ is the unit of speed). The parameter a is inversely

proportional to the width of the envelope. This solution propagates without any external driving force, as the system is energy-conserving.

The three components of $\boldsymbol{m}$ are obtained from ψ as $m_x = \sqrt{1-|\psi|^2} \equiv \psi_x$, $m_y = \mathrm{Re}\psi \equiv \psi_y$, and $m_z = -\mathrm{Im}\psi \equiv \psi_z$. The profiles of m_x and m_z are plotted in Fig. 1(b) for $a = b = 1$. From Eq. (3) and Fig. 1(b), m_x behaves as a dark soliton with amplitude $1-\sqrt{1-C^2}$ without oscillation, whereas $m_{y,z}$ behave as bright solitons precessing with circular frequency ω_0/t_0.

The analytical solution Eq. (3) is an exact solution of the nonlinear Schrödinger equation (2), which is valid only if the three assumptions above can be justified. Thus, we aim to determine to what extent the solution remains valid in the LLG dynamics, with the intact demagnetization field, nonlinear terms, and damping. To do this, the analytical solution Eq. (3) at $t = 0$

$$\psi(x',0) = C(a)\,\mathrm{e}^{\mathrm{i}bx'}\,\mathrm{sech}(ax' - \ln(2C(a))) \tag{4}$$

is set as the initial state, and the MuMax3 package[35] is used to simulate the LLG equation (1) to examine the time evolution of the initial state and compare it with the expected solution (3). The parameters are chosen as $B_0 = 0$, $A = 12$ pJ/m, and $\lambda = 8$. The nanowire has dimensions 2048 nm × 1 nm × 1 nm, and the mesh size is 1 nm × 1 nm × 1 nm, which is sufficiently small compared with the exchange length scale $x_0 \approx 5.08$ nm. Figure 2(a) shows the density plots of the m_x component for fixed $b = 1$, $a = 0.1$ (left) and 1.4 (right) in the x–t plane for $\alpha = 0$, 0.0001, and 0.001. For brevity and better comparison, we artificially stack the results for different α in the same subfigure for clarity. All solitons move at the same constant speed in each subfigure. The soliton amplitude increases while its width decreases as α increases. For $\alpha = 0.001$, the soliton amplitude decays significantly in both cases. However, for $\alpha = 0.0001$, within the micrometer length scale and nanosecond time scale, the decay is negligible. Since the damping of magnetic insulators such as YIG can be as low as 10^{-5},[36] the soliton decay is acceptable within a length scale of several micrometers. The dashed line in each subfigure represents the analytical relation $x = 2bv_0t$, where the speed $2bv_0 = 1932$ m/s is quite high for nano-devices. We can see that for $a = 0.1$, the simulated speed almost coincides with the analytical prediction, whereas for $a = 1.4$, the resulting speed is slower. This is understandable because for $a = 1.4$, the amplitude $C = 0.96$ is already very large, so the neglect of higher-order nonlinearity leads to a more significant deviation from the analytical solution. We further compare the simulated speed v for different a and α in Fig. 2(b) for fixed $b = 1$. For small amplitudes, the deviation from the analytical value is small, while the deviation increases with a. Moreover, larger damping slightly accelerates the soliton motion. We then compare the detailed magnetization profiles of the solitons. In Fig. 2(c), numerical results of the three magnetization components at 0.2 ns are plotted as symbols, and solid lines denote the analytical solutions. Here, because the speed is not precisely $2bv_0$, a properly shifted X_0 is used solely for profile comparison. For $a = 0.1$, the agreement between the numerical and analytical profiles is excellent. For $a = 1.4$, the agreement remains good, though the discrepancy is more apparent than in the case of $a = 0.1$.

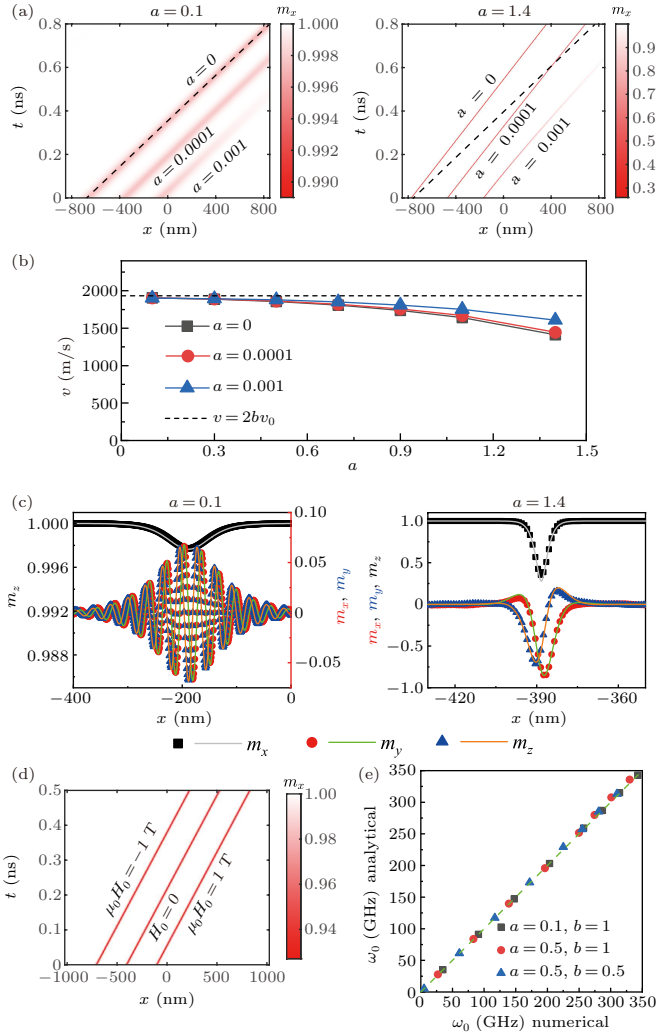


Fig. 2. (a) Density plots of m_x in the x–t plane for $b = 1$ and different a: 0.1 (left) and 1.4 (right). (b) Soliton speed for different a and damping α. Symbols denote numerical results, and the dashed line represents the theoretical value $v = 2bv_0$. (c) Magnetization profiles at 0.2 ns for $b = 1$ and different a: 0.1 (left) and 1.4 (right). Symbols are numerical data, and solid lines correspond to the analytical formula. (d) Density plots of m_x for different external fields H. (e) Comparison of the precession frequency for different a and b. The horizontal and vertical axes show numerical and analytical results, respectively, with the green dashed line indicating $y = x$.

According to the analytical solution, the longitudinal magnetic field B_0 does not affect the soliton shape and speed but changes the precession frequency ω_0. In Fig. 2(d), we vary B_0 ($B_0 = -1$ T, 0, 1 T) and simulate the evolution starting from the initial state with $a = 0.5$ and $b = 1$, and plot the numerical data together in the same figure. The three solutions ex-

hibit nearly identical m_x components. We further compare the precession frequency of $m_{y,z}$. In Fig. 2(e), the horizontal axis shows the precession frequencies obtained from the Fourier transform of the numerical data, while the vertical axis represents the analytical formula $\omega_0 = b_0 + \lambda + \frac{1}{2} - (a^2 - b^2)$. The agreement between theory and simulation is excellent.

To summarize this subsection, the analytical solution Eq. (3) of the nonlinear Schrödinger equation (as an approximation of the LLG equation) is compared with the full numerical simulation results. The deviation from the analytical solution, manifested mainly in the slower propagation speed, becomes larger when the soliton amplitude increases, which may result from neglecting the higher-order nonlinear terms. The soliton profile and the precession frequency still agree well with the analytical solution. In the following sections, we let $B_0 = 0$ and $\alpha = 0$ without loss of generality.

2.2. Reflection and refraction of magnetic solitons at an interface

We now consider the soliton propagation in a 1D nanowire heterostructure, which may be useful for device applications. There have been numerous studies on the reflection and refraction of linear spin waves, which obey a generalized Snell's law analogous to that in linear optics.[37–39] However, for nonlinear solitons, the behaviors can be markedly different. As an analogy, optical solitons, which can be described by the nonlinear Schrödinger equation[40,41] or the nonlinear Helmholtz equation,[42,43] have been intensively investigated in nonlinear optics.[44–48] The reflection and refraction of optical solitons are known to be much more complicated than those in linear media.[49–51] Therefore, it is essential to investigate the reflection and refraction behaviors of magnetic solitons.

The 1D nanowire heterostructures composed of different materials have been experimentally realized.[52] For simplicity, we consider an interface at $x = 0$ between two segments with different anisotropies, which can be tuned by an electric field[53,54] or by doping.[55] The anisotropy is λ_1 in the left half and λ_2 in the right half, while the other parameters are the same as in the previous subsection. The incident soliton is prepared by setting the initial state Eq. (4) with $a = 0.3$ and $b = 1$. Figures 3(a)–3(c) show the density plots of m_x of the incident soliton for fixed $\lambda_1 = 7$ and $\lambda_2 = 6$, 7.9, and 9, respectively. We see that for $\lambda_2 = 6$, there is almost no reflection, and the soliton enters the right half with a slightly larger speed. For $\lambda_2 = 9$, in contrast, total reflection is observed. The refracted and reflected solitons coexist when $\lambda_2 = 7.9$. Figure 3(d) summarizes the refracted (black squares) and reflected (red dots) soliton speeds for different λ_2. There is a narrow region where both refracted and reflected solitons can be clearly identified. This behavior is distinct from that of linear spin waves[37–39] (see Appendix B).

For the total refraction regime at small λ_2, we suppose that the incident $a = 0.3$, $b = 1$ soliton transforms into another soliton solution with parameters a_2 and b_2 after passing through the interface without loss. Since the nanowire is rotationally symmetric about the x axis, the x component of the total angular momentum L_x should be conserved. For a soliton with solution ψ, the x component of the angular momentum of a soliton deviating from the uniform domain is

$$L_x = \gamma^{-1} M_s S \int_{-\infty}^{\infty} (1 - \psi_x)\,\mathrm{d}x, \tag{5}$$

where S is the cross-sectional area of the nanowire. For small amplitude, employing the approximation $\psi_x = \sqrt{1 - |\psi|^2} \approx 1 - |\psi|^2/2$, the integral can be evaluated analytically as

$$\int_{-\infty}^{\infty} (1 - \psi_x)\,\mathrm{d}x \approx \int_{-\infty}^{\infty} \frac{|\psi|^2}{2}\,\mathrm{d}x = \frac{4ax_0}{\lambda + 1/2}, \tag{6}$$

thus the conservation condition gives

$$\frac{a}{\lambda_1 + 1/2} = \frac{a_2}{\lambda_2 + 1/2}. \tag{7}$$

On the other hand, in this regime, we find from the numerical data that the precession frequency ω_0 remains nearly identical on both sides of the interface, which is natural for linear waves but not necessarily true for nonlinear solitons. Thus, we have the second relation

$$\lambda_1 - (a^2 - b^2) = \lambda_2 - (a_2^2 - b_2^2). \tag{8}$$

Solving for a_2 from Eq. (7) and combining with Eq. (8), we obtain

$$b_2 = \sqrt{\lambda_1 - \lambda_2 + a^2 \left[\left(\frac{\lambda_2 + 1/2}{\lambda_1 + 1/2} \right) + 1 \right] + b^2}. \tag{9}$$

The refracted soliton speed is $2b_2 v_0$, plotted in Fig. 3(d) by the black solid line, which shows good agreement with the numerical data. In the total reflection regime at large λ_2, the reflected soliton should have $a_1 = a$ and $b_1 = -b$. The red solid line in Fig. 3(d) labels $v = -2bv_0$, and the agreement is good for large λ_2.

The radicand in Eq. (9) must be non-negative, yielding a critical value of λ_2 for total refraction, which is approximately 8.02 in this case. However, near this critical value, the behavior becomes highly complex. This complexity arises not only from the coexistence of reflection and refraction but also from the conversion into linear spin waves (as illustrated in Appendix A).

We can intuitively understand the above behaviors as follows. When an incident soliton from one region hits an interface, since it is no longer the solution for the other region, the system has to find a new solution, so reflection and refraction occur. If the anisotropy of the other section is weaker (i.e., a softer magnet), the spins therein are easily excited, so the

soliton tends to fully enter the softer region, resulting in total refraction (Fig. 3(a)). On the other hand, for a very large anisotropy (i.e., a hard magnet), it is difficult to excite the spin precession, so the soliton cannot enter the harder region, resulting in total reflection (Fig. 3(c)). In the intermediate region, the situation becomes highly complex, not only due to the coexistence of reflected and refracted solitons, but also because of the excitation of linear spin waves. In this process, the energy, angular momentum, and precession frequency are no longer conserved for the solitons because of the presence of linear spin waves. Further investigations are required to fully elucidate this behavior, which will be the subject of future studies.

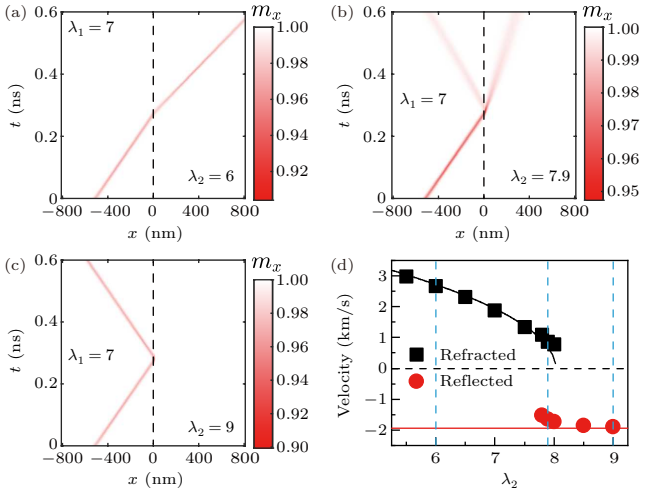


Fig. 3. Behaviors of a soliton with $a = 0.3$ and $b = 1$ propagating towards an interface at $x = 0$ from the left half with $\lambda_1 = 7$. (a)–(c) Density plots of m_x for different anisotropies of the right half: (a) $\lambda_2 = 6$, (b) $\lambda_2 = 7.9$, and (c) $\lambda_2 = 9$. (d) Dependence of refracted (black squares) and reflected (red dots) soliton speeds on the anisotropy λ_2 of the right half. Solid lines correspond to the analytical formula, and the vertical dashed lines indicate $\lambda_2 = 6$, 7.9, and 9.

2.3. Generation of magnetic solitons

Practically, it is more important to generate a soliton in an efficient and simple way. A quite intuitive idea is to use a magnetic field pulse or a spin current pulse to locally stimulate the magnetization to tilt. However, after a plethora of tests, we find that applying stimulation in a single region cannot generate a propagating soliton. Depending on the strength, direction, and duration of the stimulation, there can be irregular excitations that disperse into linear spin waves, nucleation of a new domain, or a locally precessing soliton (i.e., a soliton with $b = 0$). Propagating solitons can be generated in pairs only when stimulations of opposite directions are applied in at least two regions.

Figure 4(a) illustrates the setup of the apparatus. We apply a magnetic field $\boldsymbol{B}$ perpendicular to the wire in at least two successive regions of width w (here, we use three regions as an example). The directions of the field in adjacent regions are opposite. The magnetic field can also be replaced by a spin-polarized current injected perpendicularly into the wire. The spin polarization directions should also be opposite in adjacent regions. There can be a gap of width d between adjacent regions for practical fabrication considerations.

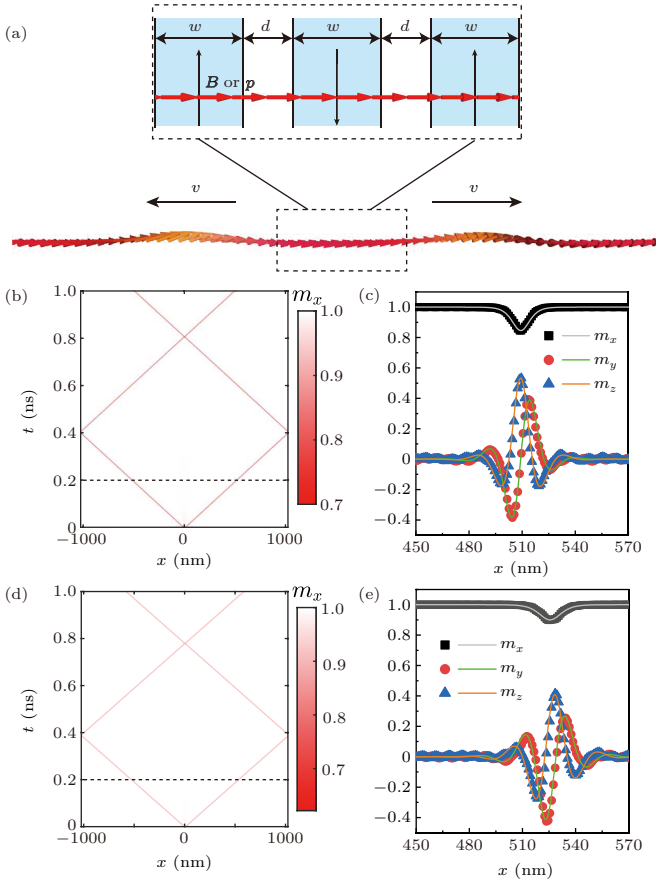


Fig. 4. (a) Schematic diagram of the soliton generation apparatus. (b) and (d) Density plots of m_x in the x–t plane showing a pair of solitons generated at the center of the wire. The dashed lines indicate 0.2 ns. (c) and (e) Magnetization profiles of the rightward-propagating soliton at 0.2 ns. Symbols represent the numerical data, and solid lines correspond to the analytical formula. (b) and (c) correspond to magnetic field stimulation, while (d) and (e) correspond to spin current stimulation.

We first consider the case in which the amplitude of the stimulation (magnetic field or spin current) in each region is the same. In this case, the overall stimulation profile is mirror-symmetric for an odd number of regions and inversion-symmetric for an even number. After applying a field pulse of large magnitude (several Tesla) but short duration ($\sim$ picoseconds), a pair of solitons can be generated, and they propagate towards opposite directions with the same speed. A typical numerical result is shown by the density plot of m_x in Fig. 4(b). The three regions of width $w = 10$ nm are placed at the center of the wire, and the separation d is 0. The material parameters are $A = 13$ pJ/m and $\lambda = 8$. The magnitude of the field pulse is $B = 4$ T and the duration is 1 ps. These parameters will be used throughout this section unless otherwise specified. It is clear that a pair of solitons is generated. The two solitons propagate in opposite directions at the same constant speed. The solitons are reflected by the

boundaries and pass through one another while maintaining the same shape, amplitude, and speed, which are typical behaviors of solitons. At 0.2 ns (the dashed line in Fig. 4(b)), we plot the magnetization profile of the right-hand side in component form (shown by symbols). The solid lines are the analytical solutions with $a = 0.777$ and $b = 1.262$, with small initial position and time shifts $X_0 = -0.47$ nm and $T_0 = 0.62$ ps, obtained by fitting the numerical data with the analytical formula. The fitted analytical profile agrees very well with the numerical data. The speed also agrees well with $v = 2bv_0 = 2538$ m/s, which is remarkably fast for ferromagnetic systems. Similarly, the soliton on the left-hand side also agrees well with the solution of $b = -1.262$, giving the same speed but in the opposite direction. If we use a spin-polarized current injected in the z direction, with a density of 1.7×10^{13} A/m^2 and polarization $P = 0.5669$, instead of the magnetic field, the results are plotted in Figs. 4(d) and 4(e). A pair of solitons with slightly larger speed and smaller amplitude ($a = 0.635$, $b = 1.317$ from fitting) is generated. In this case, the magnetization is excited via the Slonczewski spin-transfer torque.[56,57]

We further investigate how to control the generated solitons by studying the influence of material parameters (exchange constant A and anisotropy λ) as well as the stimulation conditions (stimulating field strength B and width of the stimulating region w). We choose $A = 13$ pJ/m, $\lambda = 8$, $B = 4$ T, and $w = 10$ nm as the reference parameters. Each parameter is varied while keeping the others fixed. The gap d is fixed to 0, and the pulse duration is fixed to 1 ps unless otherwise specified.

Firstly, we discuss the dependence of a and b on the material parameters A and λ. Figure 5(a) shows the variation of a (right axis) and b (left axis) with the exchange constant A. Since a stronger exchange interaction favors a more collinear magnetization alignment, the stimulated soliton amplitude, and hence a, decreases with increasing A. On the other hand, b increases with A, indicating that the stimulated solitons propagate faster for larger A. In the inset of Fig. 5(a), we plot the soliton speed and wavelength as functions of A. The wavelength $2\pi x_0/b$ (right axis) changes only slightly with A, suggesting that b is approximately proportional to $x_0 \propto \sqrt{A}$. Consequently, the soliton speed $v = 2bv_0 \propto b\sqrt{A}$ is nearly linear in A, which agrees well with the numerical results (left axis).

Figure 5(b) shows the effect of anisotropy λ on the stimulated soliton. The left axis indicates that b (and thus the wavelength and speed) is largely insensitive to λ. The parameter a exhibits a nonmonotonic dependence on λ, yet the soliton amplitude decreases with increasing λ. This behavior arises because larger anisotropy also favors a collinear magnetization alignment along x, and the m_x amplitude, given by $1 - \sqrt{1 - C^2}$, depends on both a and λ.

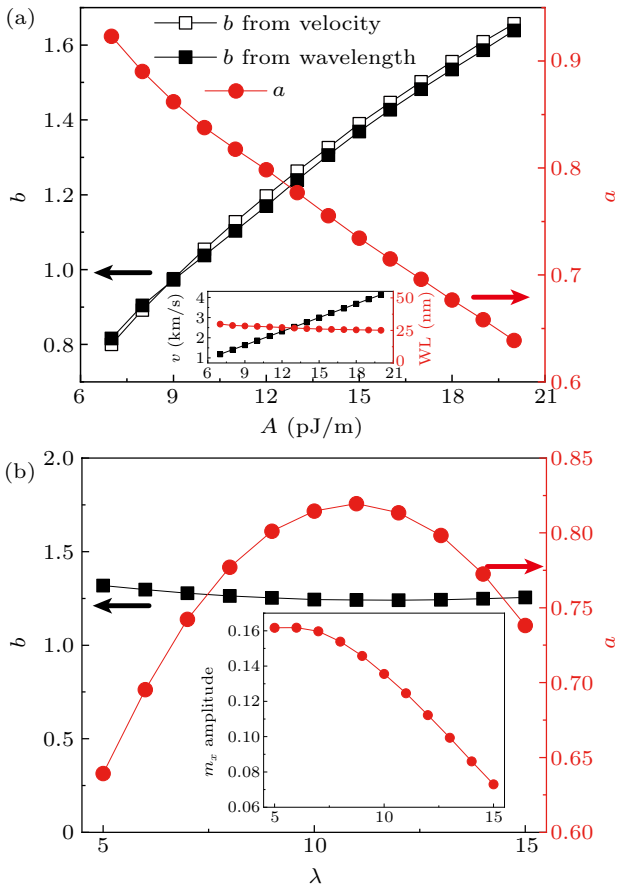


Fig. 5. (a) Dependence of b (left axis) and a (right axis) on the exchange constant A. Solid squares and hollow squares are obtained from the speed formula $v = 2bv_0$ and the wavelength $2\pi x_0/b$, respectively. Inset: dependence of the soliton speed (left axis) and wavelength (right axis) on A. (b) Dependence of b (left axis) and a (right axis) on the anisotropy λ. Inset: dependence of the soliton m_x amplitude on λ.

We then discuss the influence of the stimulation conditions on the soliton properties. Figure 6(a) shows how b (left axis) and a (right axis) vary with the stimulation field strength B. It is clear that a increases nearly linearly with the stimulation strength, while b is relatively insensitive to B, exhibiting only a slight decrease as B increases. The possible underlying reason will be discussed later.

When the region width w is altered, b and the corresponding wavelength $2\pi x_0/b$ depend on w, as shown in Fig. 6(b) by the black solid squares. The parameter b decreases with increasing region width, leading to an increase in the wavelength. We also repeat the calculations for a finite separation $d = 2$ nm and for stimulation using only two regions with $d = 0$. We find that for the same total width $w + d$, a finite separation alters b only slightly (less than 10%). In contrast, the two-region stimulation produces a smaller b, corresponding to a longer wavelength and lower speed. The variation of a with region width is shown in Fig. 6(c). Larger regions excite solitons of greater amplitude. Furthermore, a finite gap slightly reduces the soliton amplitude, whereas the two-region stimulation generates significantly weaker solitons. This explains why we adopt three-region stimulation as the representative

example in this section.

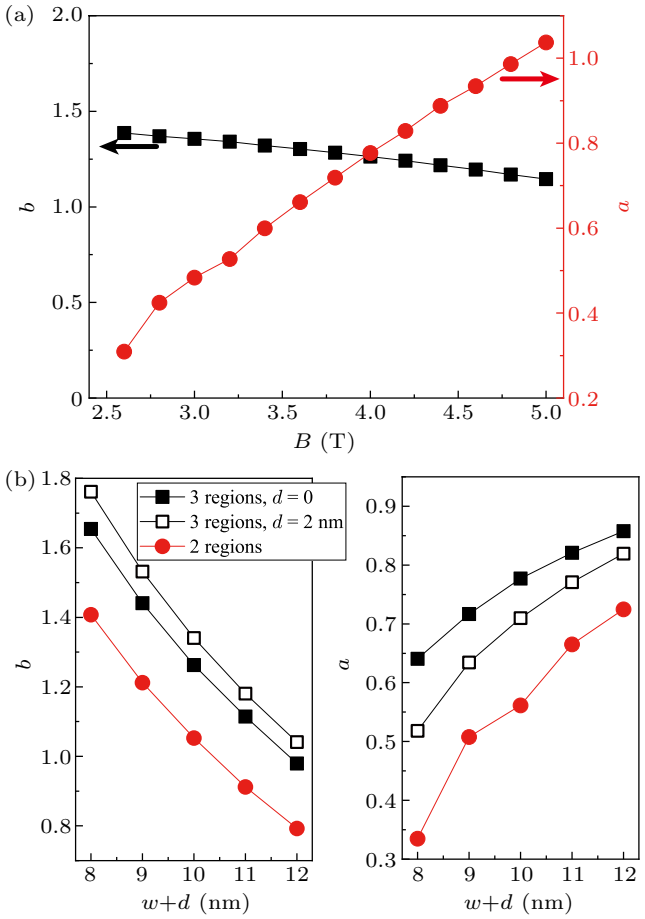


Fig. 6. (a) Dependence of b (left axis) and a (right axis) on the stimulation field strength B. (b) and (c) Dependence of b (b) and a (c) on the total stimulation width, including the region separation $w+d$. Black solid squares, black hollow squares, and red dots represent 3-region stimulation with $d=0$, 3-region stimulation with $d=2$ nm, and 2-region stimulation with $d=0$, respectively.

We next provide physical insights into the stimulation process based on the numerical results. From the analytical solution, we observe a traveling wave factor $e^{i[bx'-\omega_0(a,b)t']}$, so that within the soliton range, m_y and m_z oscillate. The alternating field pulses induce a locally oscillating magnetization profile with a wavelength larger than $2w$. Consequently, the soliton wavelength is mainly determined by the width of the stimulation region (Fig. 6(b)), and is relatively insensitive to material parameters such as A and K, as confirmed numerically in Fig. 5. Because the field directions in adjacent regions are opposite, a larger w helps release the strong exchange energy near the region boundaries, resulting in a higher soliton amplitude. However, w should not be too small; if w is close to the exchange length x_0, it becomes difficult to effectively tilt the magnetization. In addition, the soliton amplitude naturally depends on both the stimulation strength and material parameters A and K, consistent with the LLG equation.

For practical considerations, we perform further numerical tests under more realistic conditions. Replacing the square field pulse of width 1 ps with a Gaussian pulse of full width at half maximum 1 ps yields qualitatively similar results. We also examine soliton generation in magnetic strips without rotational symmetry around the x axis. For thin strips not much wider than the exchange length x_0, soliton pairs can still be excited, although the analytical solution Eq. (3) is no longer strictly valid. Note that additional excitations are inevitably generated alongside the solitons. For example, in Figs. 4(b) and 4(d), light red regions appear near the source, and in Figs. 4(c) and 4(d), oscillations persist outside the soliton range. These unwanted excitations dissipate into linear spin waves and gradually spread out. For a given soliton amplitude, two-region stimulation with stronger field or current can significantly suppress such unwanted excitations.

We then consider asymmetric stimulation by allowing different magnetic field amplitudes in the two regions shown in Fig. 7(a), where $\boldsymbol{B}_1$ ($\boldsymbol{B}_2$) in the left (right) region points along $-y$ ($+y$). The material and stimulation parameters are fixed at $A=13$ pJ/m, $\lambda=8$, $w=10$ nm, $d=0$, pulse duration 1 ps, and $B_2=6$ T. When $B_1=B_2$, symmetric soliton pairs are generated, as discussed previously. As B_1 decreases, the soliton pairs become asymmetric, and the speed of the leftward soliton decreases. For $B_1=B_2/3=2$ T, only one prominent soliton propagates rightward at a slower speed, accompanied by minor excitations. Figure 7(d) shows the magnetization profile at 1 ns, where symbols represent numerical data and solid lines are fits using the analytical solution Eq. (3) with $a=0.6221$ and $b=0.1596$. Noticeably, more significant noise is present compared to the symmetric stimulation in Fig. 4(c). For $B_1=0$, only one region is stimulated, resulting in no propagating soliton, as illustrated in Fig. 7(c).

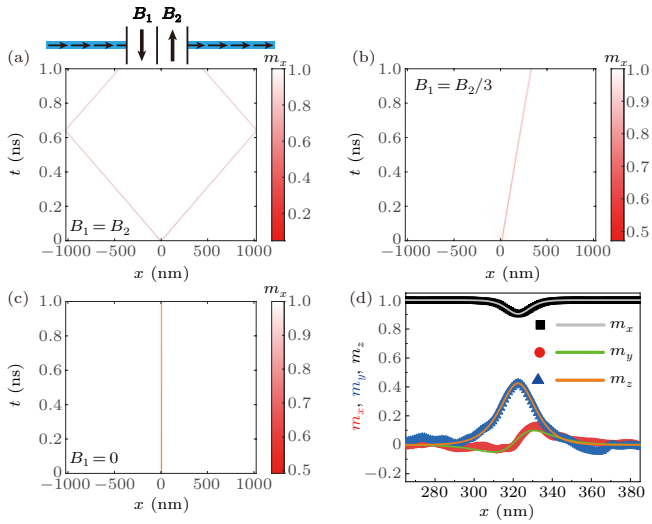


Fig. 7. (a) Set-up of two-region stimulation and the corresponding density plot of m_x for $B_1=B_2=6$ T. (b)–(c) Density plots of m_x for (b) $B_1=B_2/3$ and (c) $B_1=0$. (d) Magnetization profile at 1 ns for $B_1=B_2/3$. Symbols represent the numerical data, and solid lines are the fit using the analytical solution Eq. (3).

2.4. Discrete manipulation of domain wall by solitons

It is well known that linear spin waves can drive domain wall propagation.[33,58,59] For a uniaxial magnetic wire, the rotational symmetry around the x direction ensures the conservation of the x-component of angular momentum. Similar to linear spin waves,[33] solitons also carry a finite angular momentum. Consequently, a magnetic soliton passing through a domain wall can drive the domain wall to move in the direction opposite to soliton propagation. Due to the localized nature of the soliton, the domain wall undergoes a finite displacement ΔX after a single soliton passes through, as illustrated in Fig. 8(a) and in the animation in the supplementary material.[60]

We consider a soliton described by Eq. (3) in a wire of length L, and the m_x profile of the domain wall is $f_{\mathrm{DW}}(x - X_{\mathrm{DW}})$, where X_{DW} is the position of the domain wall center, defined as $X_{\mathrm{DW}} = \frac{1}{2}\int_{-L/2}^{L/2} f_{\mathrm{DW}}(x - X_{\mathrm{DW}})\,\mathrm{d}x$.[61] From the angular momentum conservation before and after the soliton passes through the domain wall, $\int_{-L/2}^{L/2} m_x \mathrm{d}x = \text{constant}$, we assume that the soliton and domain wall are sufficiently separated so that the integrations can be treated independently

$$\begin{aligned}&\int_{-L/2}^{L/2} f_{\mathrm{DW}}(x - X_1)\,\mathrm{d}x - \int_{-L/2}^{L/2}(1-\psi_x)\,\mathrm{d}x \\ &= \int_{-L/2}^{L/2} f_{\mathrm{DW}}(x - X_2)\,\mathrm{d}x + \int_{-L/2}^{L/2}(1-\psi_x)\,\mathrm{d}x, \end{aligned} \tag{10}$$

where X_1 and X_2 are the domain wall positions before and after soliton penetration. Therefore, the relation between the soliton profile and the domain wall displacement $\Delta X = X_2 - X_1$ is

$$\Delta X = -\int_{-L/2}^{L/2}(1-\psi_x)\,\mathrm{d}x \approx -\frac{4a}{\lambda + 1/2}x_0. \tag{11}$$

This process can occur repeatedly, leading to a discrete manipulation of the domain wall. Figure 8(b) shows the simulation result for periodically applied stimulation. The stimulation region extends from -500 nm to -470 nm with $A = 13$ pJ/m, $\lambda = 8$, $w = 10$ nm, $d = 0$, and $B = 4$ T. Outside the range -600 nm to 600 nm, the damping increases linearly from 0.0001 to 1 to absorb excitations and prevent reflections at the boundaries. The stimulation is applied for 1 ps and then ceased for 1 ns. A head-to-head domain wall and a tail-to-tail domain wall are initially placed at $x = 0$ and $x = 300$ nm, respectively. The main figure shows the density plot of m_x. Soliton pairs are generated periodically and propagate in both directions at constant speed. After passing through each domain wall, the wall shifts towards the stimulation source by a certain distance, regardless of whether it is head-to-head or tail-to-tail. The inset shows a close-up of the region indicated by the dashed frame near the domain wall, emphasizing the displacement.

We then vary the stimulation strength B to generate solitons of different amplitudes, and record the displacements ΔX from the numerical results by locating $m_x = 0$ after interpolation. Comparison with the analytical formula Eq. (11) in Fig. 8(c) shows good agreement.

The discrete manipulation of domain walls is highly useful in device applications such as racetrack memory,[4] where precise control of domain wall positions is essential. Our method provides natural discrete control of domain wall positions and does not require complicated pinning apparatuses, as in continuous-source-driven domain wall motion.[62] In addition, achieving a strong magnetic field of several Teslas or a current of 10^{13} A/m^2 for 1 ps is experimentally feasible.

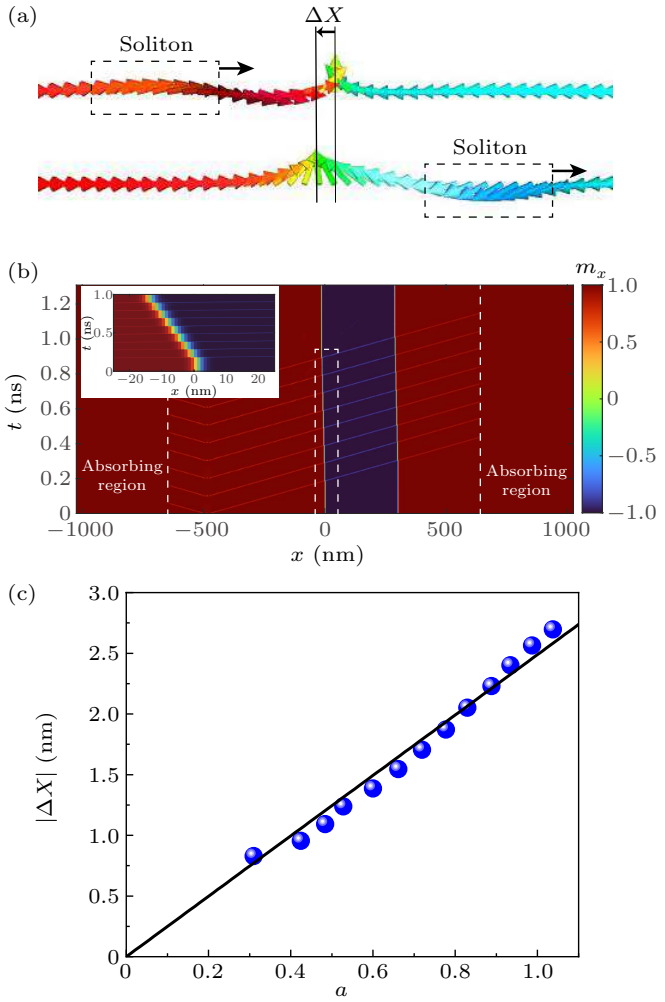


Fig. 8. (a) Schematic diagram of a soliton passing through a domain wall. (b) Density plot of m_x in the x–t plane. Two domain walls are initially placed at the center and at $x = 300$ nm. Solitons are stimulated in the region -500 to -470 nm with a period of 0.101 ns. Inset: close-up view near the domain wall. (c) Comparison between the domain wall shift obtained from numerical data (symbols) and the analytical formula $|\Delta X| = 4ax_0/\left(\lambda + \frac{1}{2}\right)$ (solid line).

3. Discussion and summary

Topologically trivial magnetic solitons exhibit unique properties distinct from well-studied topologically nontrivial solitons and linear spin waves. Unlike linear spin waves, which experience dispersion, topologically trivial solitons propagate while maintaining their localized envelope. More-

over, their precession frequency and 'wavenumber' are not linked by a dispersion relation. In contrast to nontrivial solitons, such as domain walls and skyrmions, whose structures are nearly rigid, trivial solitons possess internally oscillatory components, making the Thiele equation[63] inapplicable.

To study the response of trivial solitons to external driving, we apply a longitudinal spin-polarized current to a soliton, considering the adiabatic spin transfer torque[64] $\boldsymbol{\tau} = v_j \partial \boldsymbol{m}/\partial x$, where $v_j = P j \mu_B/(eM_s)$ (μ_B is the Bohr magneton, j is the current density, e is the electron charge, and P is the spin polarization). In the presence of this torque (with $\alpha = 0$), the soliton velocity changes from $2bv_0$ to $2bv_0 + v_j$.[23] If the current is turned on suddenly, the velocity changes abruptly, indicating inertialess dynamics. In this sense, the soliton studied here can be considered massless. A typical result is presented in Appendix C.

One-dimensional solitons may be experimentally observed in thin magnetic nanostrips. We have numerically verified that the results are qualitatively valid for strip widths up to about $2x_0$ ($\sim$10 nm for the parameters used). For materials with larger exchange strength, this width can be greater and potentially fabricated.[52,65] Imaging of the soliton can be performed using techniques such as x-ray magnetic circular dichroism[66] or nitrogen-vacancy center magnetometry.[67,68] The precession frequency can also be measured indirectly.[69] The measured amplitude, speed, and frequency directly correspond to a and b in our theoretical model, allowing experimental verification.

In summary, the analytical solution of magnetic solitons, obtained using the shape anisotropy approximation, neglecting damping, and assuming small amplitude, agrees well with numerical simulations of the full LLG equation for reasonably low damping and small amplitudes. When a soliton enters another wire segment with different anisotropy, it exhibits total refraction for weak anisotropy and total reflection for strong anisotropy, with angular momentum and precession frequency approximately conserved. Near a critical intermediate anisotropy, soliton behavior becomes more complex, with coexistence of reflection and refraction, and conversion into linear spin waves.

Pairs of magnetic solitons can be generated by magnetic field or spin-polarized current pulses applied to at least two successive regions with alternating directions. The opposing directions create a locally oscillating magnetization profile resembling the soliton profile, allowing solitons to propagate in opposite directions. Three-region stimulation produces larger amplitudes than two-region stimulation under otherwise identical conditions. Soliton properties can be tuned by adjusting stimulation parameters. When a magnetic soliton passes through a domain wall, it drives the wall to shift opposite to the soliton propagation direction, regardless of whether the wall is head-to-head or tail-to-tail. The displacement can be accurately described by angular momentum conservation. These findings enable discrete manipulation of domain walls and provide a paradigm for magnetic soliton-based devices.

Appendix A: A soliton converting to a refracted soliton and a reflected linear spin wave packet

Here we present a typical example in which a soliton refracts as another soliton but reflects as a linear spin wave packet. Figure A1 shows the case with $\lambda_1 = 7$, $\lambda_2 = 5.5$, and an incident soliton with $a = 0.5$ and $b = 0.5$. The density plot of m_x in (a) and the snapshots at different times in (b) show that the refracted portion remains a soliton, whereas the reflected portion exhibits clear dispersion, indicating it forms a linear spin wave packet. The conversion of solitons into linear spin waves is ubiquitous in the numerical studies presented in Subsection 2.2. However, for relatively weak or strong λ_2 values far from the critical point, the dissipation into linear spin waves is negligible.

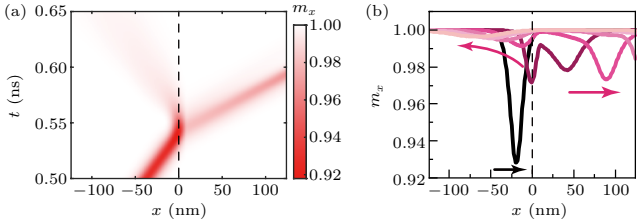


Fig. A1. (a) Density plot of m_x in the x–t plane near the interface for $\lambda_1 = 7$, $\lambda_2 = 5.5$, with an incident soliton of $a = 0.5$ and $b = 0.5$. (b) Snapshots of m_x showing the incident soliton (black line) and the profiles after passing the interface (pink lines with varying brightness). Brighter lines correspond to later times.

Appendix B: Reflection and refraction of a linear spin wave in 1D

For a linear spin wave, the nonlinear term in Eq. (2) is neglected. Thus, the reflection and refraction of a 1D spin wave at an interface between regions of different anisotropy are analogous to an electron encountering a step potential. The dispersion relation of linear spin waves is

$$\omega = \frac{2\gamma}{M_s}\left(Ak^2 + K\right). \tag{B1}$$

We assume that the incident spin wave is $c_0 e^{i(kx-\omega t)}$, the reflected wave is $c_1 e^{i(-kx-\omega t)}$, and the refracted wave is $c_2 e^{i(k'x-\omega t)}$. The continuity conditions (i.e., ψ and $\partial_x \psi$ are continuous) then give $c_0 + c_1 = c_2$ and $kc_0 - kc_1 = k'c_2$. Thus, the amplitudes of the reflected and refracted spin waves are

$$c_1 = \frac{k'-k}{k'+k}c_0, \quad c_2 = \frac{2k}{k'+k}c_0. \tag{B2}$$

For the $a = 0.3$, $b = 1$ soliton discussed in Fig. 3, the precessing frequency is $\omega_0 = (\gamma\mu_0 M_s)[\lambda_1 - (a^2 - b^2)]$. For a linear spin wave with the same frequency, the incident wavevector k

is $0.188x_0^{-1}$. For $\lambda_2 = 6$, $k' = 0.272x_0^{-1}$, so the reflected amplitude $c_1 = -0.183$. This differs from the nearly invisible reflection observed in Fig. 3(a). Also, the threshold λ_2 for total reflection is $\lambda_2 > \lambda_1 - (a^2 - b^2) = 7.91$ (k' becomes imaginary), which also differs from the value 8.02 obtained for solitons. This is evident from the data point at $\lambda_2 = 8$ in Fig. 3(d), where significant refraction is still observed. Since linear spin waves are extended rather than localized, their reflection and refraction cannot be visualized as density plots like in Fig. 3.

Appendix C: Dynamics of a soliton under adiabatic spin transfer torque

Here, we use the same material parameters as those in Fig. 2(b), and α is set to 0. We use an $a = 0.3$, $b = 1$ soliton as the initial state, and a fully polarized current of $j = 10^{13}$ A/m^2 ($v_j = 674.0$ m/s) is switched on at 0.5 ns. The position of the soliton is shown in Fig. C1. The inset shows a close-up around 0.5 ns, with the time step chosen to be less than 1 ps. The sharp change in slope indicates that the soliton velocity changes abruptly, without any gradual acceleration. Further investigations into the driven dynamics of topologically trivial solitons are warranted.

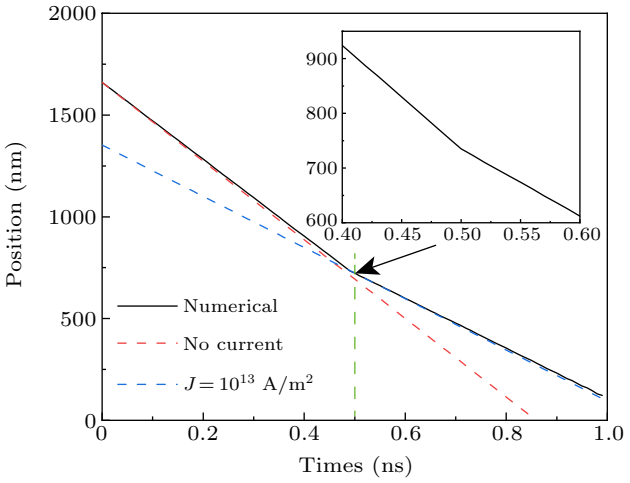


Fig. C1. Motion of a soliton with $a = 0.3$ and $b = 1$, driven by adiabatic spin transfer torque turned on at 0.5 ns with $\alpha = 0$. The solid line represents the numerical result, and the dashed line shows the prediction from the analytical formula. Inset: close-up near 0.5 ns.

Acknowledgments

Project supported by the National Natural Science Foundation of China (Grants Nos. 11804045 and 12174093), the Natural Science Foundation of Hunan Province of China (Grant No. 2025JJ60001), and the Fundamental Research Funds for the Central Universities.

References

[1] Lin X, Yang W, Wang K L and Zhao W 2019 *Nat. Electron.* **2** 274
[2] Hirohata A, Yamada K, Nakatani Y, Prejbeanu I L, Diény B, Pirro P and Hillebrands B 2020 *J. Magn. Magn. Mater.* **509** 166711
[3] Noël P, Trier F, Vicente Arche L M, Bréhin J, Vaz D C, Garcia V, Fusil S, Barthélémy A, Vila L, Bibes M and Attané J P 2020 *Nature* **580** 483
[4] Parkin S S P, Hayashi M and Thomas L 2008 *Science* **320** 190
[5] Zhang X, Zhao G P, Fangohr H, Liu J P, Xia W X, Xia J and Morvan F J 2015 *Sci. Rep.* **5** 7643
[6] Allwood D A, Xiong G, Faulkner C C, Atkinson D, Petit D and Cowburn R P 2005 *Science* **309** 1688
[7] Luo S, Song M, Li X, Zhang Y, Hong J, Yang X, Zou X, Xu N and You L 2018 *Nano Lett.* **18** 1180
[8] Luo Z, Hrabec A, Dao T P, Sala G, Finizio S, Feng J, Mayr S, Raabe J, Gambardella P and Heyderman L J 2020 *Nature* **579** 214
[9] Jiao X, Wang X S and Lan J 2024 *Phys. Rev. B* **109** 094428
[10] Wang X S and Wang X R 2021 *Topology in Magnetism* (Chambridge: Springer International Publishing) pp. 357–403
[11] Nagaosa N and Tokura Y 2013 *Nat. Nanotechnol.* **8** 899
[12] Thiaville A and Miltat J 2018 *Topology and Magnetic Domain Walls* (Chambridge: Springer International Publishing) pp. 41–73
[13] Ma X P, Ai X, Yang X X, Cai M X, Shim J H and Piao H G 2023 *J. Magn. Magn. Mater.* **581** 170665
[14] Wang X S, Qaiumzadeh A and Brataas A 2019 *Phys. Rev. Lett.* **123** 147203
[15] Jing K Y, Sun Z Z and Wang X R 2024 *Phys. Rev. B* **110** 054414
[16] de Assis I R, Mertig I and Göbel B 2024 *Phys. Rev. B* **110** 064404
[17] Liu Y and Nagaosa N 2024 *Phys. Rev. Lett.* **132** 126701
[18] Zang J, Mostovoy M, Han J H and Nagaosa N 2011 *Phys. Rev. Lett.* **107** 136804
[19] Hayashi M, Thomas L, Rettner C, Moriya R, Bazaliy Y B and Parkin S S P 2007 *Phys. Rev. Lett.* **98** 037204
[20] Jiang W, Upadhyaya P, Zhang W, Yu G, Jungfleisch M B, Fradin F Y, Pearson J E, Tserkovnyak Y, Wang K L, Heinonen O, te Velthuis S G E and Hoffmann A 2015 *Science* **349** 283
[21] Kosevich A, Ivanov B and Kovalev A 1990 *Phys. Reports* **194** 117
[22] Jiang S, Chung S, Ahlberg M, Frisk A, Khymyn R, Le Q T, Mazraati H, Houshang A, Heinonen O and Åkerman J 2024 *Nat. Commun.* **15** 2118
[23] Li Z D, He P B and Liu W M 2014 *Chin. Phys. B* **23** 117502
[24] Mohseni S M, Sani S R, Persson J, Nguyen T N A, Chung S, Pogoryelov Y, Muduli P K, Iacocca E, Eklund A, Dumas R K, Bonetti S, Deac A, Hoefer M A and Åkerman J 2013 *Science* **339** 1295
[25] Backes D, Maci'a F, Bonetti S, Kukreja R, Ohldag H and Kent A D 2015 *Phys. Rev. Lett.* **115** 127205
[26] Maci'a F, Backes D and Kent A D 2014 *Nat. Nanotechnol.* **9** 992
[27] Giridharan D, Sabareesan P and Daniel M 2016 *Phys. Rev. E* **94** 032222
[28] Daniel M and Beula J 2008 *Phys. Rev. B* **77** 144416
[29] Li Z D, Cui H, Li Q Y and He P B 2018 *Ann. Phys.* **388** 390
[30] Li Z D, Bao Q L, He P B, Xu T F and Wu B 2020 *J. Magn. Magn. Mater.* **512** 166981
[31] Zhao Y M, Jin X W and Yang Z Y 2023 *New J. Phys.* **25** 113029
[32] Jin X W, Yang Z Y, Liao Z M, Jing G and Yang W L 2024 *Phys. Rev. B* **109** 014414
[33] Yan P, Wang X S and Wang X R 2011 *Phys. Rev. Lett.* **107** 177207
[34] Ma W X 2022 *Partial Differ. Equ. Appl. Math.* **5** 100220
[35] Vansteenkiste A, Leliaert J, Dvornik M, Helsen M, Garcia-Sanchez F and Van Waeyenberge B 2014 *AIP Adv.* **4** 107133
[36] Hauser C, Richter T, Homonnay N, Eisenschmidt C, Qaid M, Deniz H, Hesse D, Sawicki M, Ebbinghaus S G and Schmidt G 2016 *Sci. Rep.* **6** 20827
[37] Stigloher J, Decker M, Körner H S, Tanabe K, Moriyama T, Taniguchi T, Hata H, Madami M, Gubbiotti G, Kobayashi K, Ono T and Back C H 2016 *Phys. Rev. Lett.* **117** 037204
[38] Mulkers J, Van Waeyenberge B and Milošević M V 2018 *Phys. Rev. B* **97** 104422
[39] Yu W, Lan J, Wu R and Xiao J 2016 *Phys. Rev. B* **94** 140410
[40] Hasegawa A and Tappert F 1973 *Appl. Phys. Lett.* **23** 142
[41] Hasegawa A and Tappert F 1973 *Appl. Phys. Lett.* **23** 171
[42] Chamorro-Posada P and McDonald G S 2003 *Opt. Lett.* **28** 825
[43] Christian J M, McDonald G S, Potton R J and Chamorro-Posada P 2007 *Phys. Rev. A* **76** 033834
[44] Gibbon J D and Eilbeck J C 1972 *J. Phys. A* **5** L122
[45] Caudrey P J, Eilbeck J C, Gibbon J D and Bullough R K 1973 *J. Phys. A* **6** L112
[46] Boardman A 1997 *Nature* **387** 854

[47] Maimistov A I 2010 *Quantum Electron.* **40** 756
[48] LIN X G, LIU W J and LEI M 2016 *Pramana* **86** 575
[49] Sánchez-Curto J, Chamorro-Posada P and McDonald G S 2007 *Opt. Lett.* **32** 1126
[50] Sánchez-Curto J, Chamorro-Posada P and McDonald G S 2010 *Opt. Lett.* **35** 1347
[51] Kominis Y and Hizanidis K 2009 *Phys. Rev. Lett.* **102** 133903
[52] Hyun J K, Zhang S and Lauhon L J 2013 *Ann. Rev. Mater. Res.* **43** 451
[53] Wang C T, Liang X F, Zhang Y, Liang X, Zhu Y P, Qin J, Gao Y, Peng B, Sun N X and Bi L 2017 *Phys. Rev. B* **96** 224403
[54] Deka A, Rana B, Anami R, Miura K, Takahashi H, Otani Y and Fukuma Y 2020 *Phys. Rev. B* **101** 174405
[55] Matsukura F, Tokura Y and Ohno H 2015 *Nat. Nanotechnol.* **10** 209
[56] Slonczewski J 1996 *J. Magn. Magn. Mater.* **159** L1
[57] Berger L 1996 *Phys. Rev. B* **54** 9353
[58] Han J, Zhang P, Hou J T, Siddiqui S A and Liu L 2019 *Science* **366** 1121
[59] Wang Y, Zhu D, Yang Y, Lee K, Mishra R, Go G, Oh S H, Kim D H, Cai K, Liu E, Pollard S D, Shi S, Lee J, Teo K L, Wu Y, Lee K J and Yang H 2019 *Science* **366** 1125
[60] See supplementary material for an animation of a soliton passing through a domain wall.
[61] Porter D G and Donahue M J 2004 *J. Appl. Phys.* **95** 6729
[62] Yuan H Y and Wang X R 2014 *Phys. Rev. B* **89** 054423
[63] Thiele A A 1973 *Phys. Rev. Lett.* **30** 230
[64] Zhang S and Li Z 2004 *Phys. Rev. Lett.* **93** 127204
[65] Vázquez M 2020 *Magnetic Nano- and Microwires: Design, Synthesis, Properties and Applications: Woodhead Publishing Series in Electronic and Optical Materials* (Elsevier Science)
[66] Bonetti S, Kukreja R, Chen Z, Macià F, Hernàndez J M, Eklund A, Backes D, Frisch J, Katine J, Malm G, Urazhdin S, Kent A D, Stöhr J, Ohldag H and Dürr H A 2015 *Nat. Commun.* **6** 8889
[67] van der Sar T, Casola F, Walsworth R and Yacoby A 2015 *Nat. Commun.* **6** 7886
[68] Dovzhenko Y, Casola F, Schlotter S, Zhou T X, Büttner F, Walsworth R L, Beach G S D and Yacoby A 2018 *Nat. Commun.* **9** 2712
[69] Turenne D, Yaroslavtsev A, Wang X, *et al.* 2022 *Sci. Adv.* **8** eabn0523